# MEASUREMENT-BASED MODAL BEAMFORMING USING PLANAR CIRCULAR MICROPHONE ARRAYS

*Markus Zaunschirm*
Institute of Electronic Music and Acoustics
Univ. of Music and Performing Arts Graz
Graz, Austria
zaunschirm@iem.at

*Franz Zotter*
Institute of Electronic Music and Acoustics
Univ. of Music and Performing Arts Graz
Graz, Austria
zotter@iem.at

**ABSTRACT**

This paper describes how to use a planar circular pressure-zone table-top microphone array for modal beamforming. Its goals are similar as for spherical arrays: higher-order resolution and a more-or-less steering-invariant beampattern design in the three-dimensional half space. As conventional circular arrays lack control of the beampattern in the vertical array plane, the proposed arrangement tries to fix this shortcoming to allow both horizontal and vertical control of beamforming. To provide a fully calibrated decomposition into the directional modes, the proposed beamforming approach is based on measurement data. From a MIMO (multiple-input-multiple-output) system description of the measurement data in the spherical harmonics domain, an inverse MIMO system of filters is designed for decomposing the microphone array signals into those spherical components eligible for modal beamforming. For an efficient measurement and robust set of decomposition filters, a reduced set of measurement positions and a regularisation strategy is suggested.

## 1. INTRODUCTION

Beamforming denotes the discrimination between signals based on the spatial location of sources. Whilst conventional beamforming algorithms directly operate on the sensor signals, modal beamforming approaches use directional modes that are obtained by decomposing the wavefield into orthogonal solutions of the acoustic wave equation. Overviews are given in [1, 2].

Spherical arrays are most generic, but also require a lot of hardware effort. In real-world scenarios where acoustic sources are restrained to the upper half of the three-dimensional space the geometry of the microphone array needs to be adopted. For example Li and Duraiswami [3] designed a hemispherical table microphone for sound capture and beamforming. In order to further decrease cost and hardware complexity, circular planar microphone arrays are feasible. In [4] a planar circular table microphone array, consisting of three near-coincident cardioid microphones, is presented that allows for decomposition of the acoustic scene in modes of first order. Using this setup looses its directivity when steering the spatial sensitivity into the vertical direction. In order to improve the spatial selectivity of the generated beampattern, a higher order resolution is required. An approach for a decomposition of the soundfield in second-order directional modes is outlined in literature by Meyer and Elko in [5] and [6]. They suggest a microphone array consisting of omnidirectional microphones on a concentric circle and an omnidirectional centre element. Craven et al [7] argue that acoustic gradient sensors are preferable in signal to noise behaviour as they decrease the bass boosts of array processing filters. On the other hand manufacturing of cardioid microphones usually does not yield capsules that are as well-matched as omnidirectional ones, although a precise match is required for accurate array processing. Additionally, the orientation of the cardioid microphones needs to be precise in order to avoid mismatch between analytic model and prototype. This paper describes how to obtain a fully calibrated decomposition

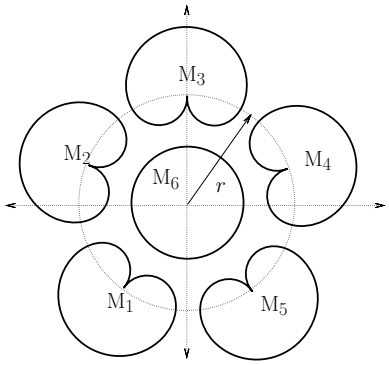


Figure 1: *Schematic layout of the prototype.*

into the directional modes, and a beamforming approach that is entirely based on measurement data and does not rely on an analytic model. A schematic layout of the used microphone array is depicted in figure 1. The central element is an omnidirectional microphone and five equi-spaced outwards-oriented cardioid microphones lie on a concentric circle of the radius r. The array is planar and intended for use as a pressure-zone microphone that is placed for example on table. Possible applications include beamforming for teleconferencing and to a certain extent also 3D spatial recordings.

## 2. MEASUREMENTS OF MICROPHONE ARRAY CHARACTERISTICS

The directional sensitivity of the six array microphones can be measured for one direction by recording a sweep from a loudspeaker that is placed there. For a complete measurement of as many directional responses as possible, the direction-dependent response of each microphone is measured by a hemispherically surrounding loudspeaker array.

Measurement excitation positions (loudspeaker positions) are set according to a spatial resolution of $\Delta\varphi = 10^\circ$ in azimuth and $\Delta\vartheta = 11.25^\circ$ in zenith direction which leads to a grid layout of 8

latitude circles and 36 meridians. The right half of fig. 2 depicts the hemispherical measurement configuration of 288 loudspeakers on a radius of $1.3m$. In order to reduce the measurement effort, the number of directions may be reduced to 6 instead of 288, see red dots in the right half of fig. 2. In the practical setup, fig. 2, an eight-element quarter-circular loudspeaker array could be used for sequentially measuring 8 directions of different zenith angles at one azimuth angle. In order to reach all 36 proposed azimuth angles, the microphone array is rotated by a computer-controlled turntable between the measurements.

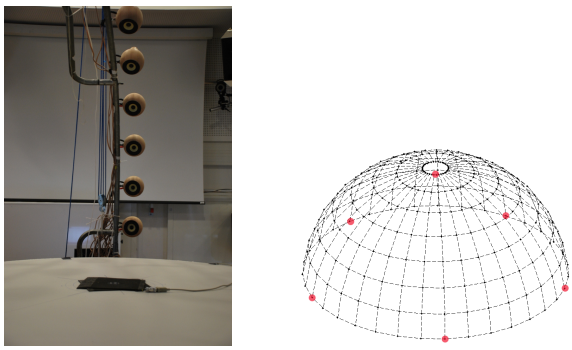

Figure 2: *Setup for capturing responses on a* $8 \times 36$ *longitude/latitude grid; red dots mark the on-axis directions.*

The measurements span an $8 \times 36$ set of impulse responses $h_{\lambda\mu}[\tau]$, where $\lambda$, $\mu$ and $\tau$ are the loudspeaker, microphone and discrete-time indices, respectively.

The actual measurements are done according to the exponentially swept-sine (ESS) method presented by Farina in [8]. The impulse responses between the $\lambda^{\text{th}}$ loudspeaker to the $\mu^{\text{th}}$ microphone are calculated in the frequency domain by a simple division of the two spectra defined in eq. (1)

$$h_{\lambda\mu}[\tau] = IFFT\left[\frac{FFT(x_{\lambda\mu}[\tau])}{FFT(s[\tau])}\right], \tag{1}$$

where $x_{\lambda\mu}[\tau]$ and $s[\tau]$ denote the recorded response and the exponential sweep, respectively. The influences of the loudspeaker characteristics are minimized by equalizing according to a calibrated reference microphone placed in the centre of the experimental setup.

### 2.1. Directivity patterns

In this section, we analyse the measurement data in order to make a statement about the three dimensional directivity patterns and their rotational symmetry of the analysed microphones. Let us define a vector that contains the discrete directional response of the $\mu^{\text{th}}$ microphone ($\mu = 1, \ldots, 6$) as

$$\boldsymbol{h}_\mu(\omega) = \begin{pmatrix} h_\mu(\boldsymbol{\theta}_1, \omega) \\ h_\mu(\boldsymbol{\theta}_2, \omega) \\ \vdots \\ h_\mu(\boldsymbol{\theta}_{\text{L}}, \omega) \end{pmatrix}, \tag{2}$$

where $\boldsymbol{\theta}_\lambda = [\cos(\varphi_\lambda)\sin(\vartheta_\lambda),\ \sin(\varphi_\lambda)\sin(\vartheta_\lambda),\ \cos(\vartheta_\lambda)]^{\text{T}}$ is a direction vector using the azimuth and zenith angle $\varphi_\lambda$ and $\vartheta_\lambda$ of the $\lambda^{\text{th}}$ loudspeaker ($\lambda = 1, \ldots, \text{L}$) in spherical coordinates. The magnitude of the directivity pattern at a specific frequency is then plotted using a spherical meshgrid of the available grid positions in fig. 3.

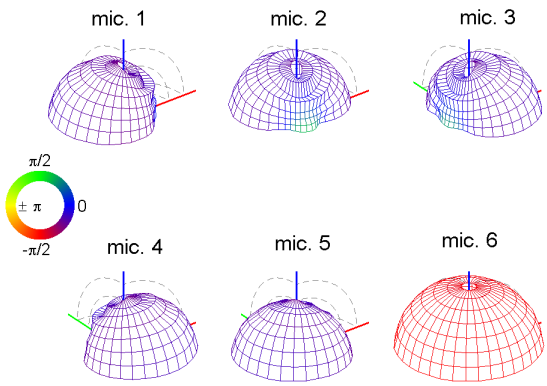


Figure 3: *Directivity patterns of mounted microphones at* $f \approx 1\,\text{kHz}$ *on the* $8 \times 36$ *measurement grid; color expresses the phase.*

### 2.2. Directivity patterns in modal domain

From the series of L loudspeaker responses to the $\mu^{\text{th}}$ microphone, we obtain a single response by linear combination of all loudspeakers with the weight $\boldsymbol{g} = [g_1, \ldots, g_{\text{L}}]^{\text{T}}$

$$h_\mu(\omega) = \boldsymbol{h}_\mu^{\text{T}}(\omega)\,\boldsymbol{g}. \tag{3}$$

As a counterpart to the weight vector of the spaced loudspeakers at their discrete locations, we define a continuous driving distribution $g(\boldsymbol{\theta})$ depending on the direction vector $\boldsymbol{\theta}$. Such a function is related to the loudspeaker weights $g_\lambda$ by

$$g(\boldsymbol{\theta}) = \sum_{\lambda=1}^{\text{L}} \delta(\boldsymbol{\theta} - \boldsymbol{\theta}_\lambda)\, g_\lambda, \tag{4}$$

$\delta(\boldsymbol{\theta} - \boldsymbol{\theta}_\lambda)$ symbolizing the directional Dirac delta function. For a modal representation, the equation is expanded in spherical harmonics $Y_n^m(\boldsymbol{\theta})$

$$g(\boldsymbol{\theta}) = \sum_{n=0}^{\infty} \sum_{m=-n}^{n} \underbrace{\sum_{\lambda=1}^{\text{L}} Y_n^m(\boldsymbol{\theta}_\lambda)\, g_\lambda}_{:=\gamma_n^m}\, Y_n^m(\boldsymbol{\theta}), \tag{5}$$

$Y_n^m(\boldsymbol{\theta}_\lambda)$ being the expansion coefficients of the Dirac delta function and $\gamma_{nm}$ of their weighted superposition. The resolution of $g(\boldsymbol{\theta})$ is limited by truncating the summation in $n$ to $n \leq \text{N}$, a number of functions we can resolve by the measurement loudspeakers. In terms of matrices and vectors, we may write instead of $\gamma_n^m = \sum_{\lambda=1}^{\text{L}} Y_n^m(\boldsymbol{\theta}_\lambda)\, g_\lambda$

$$\begin{aligned} \boldsymbol{\gamma}_{\text{N}} = \boldsymbol{L}_{\text{N}}\,\boldsymbol{g}, \qquad & \text{with } \boldsymbol{L}_{\text{N}} = [\boldsymbol{y}_{\text{N}}(\boldsymbol{\theta}_1),\ \ldots,\ \boldsymbol{y}_{\text{N}}(\boldsymbol{\theta}_{\text{L}})], \\ & \boldsymbol{y}_{\text{N}}^{\text{T}}(\boldsymbol{\theta}) = [Y_0^0(\boldsymbol{\theta}),\ \ldots, Y_{\text{N}}^{\text{N}}(\boldsymbol{\theta})], \\ & \text{and } \boldsymbol{\gamma}_{\text{N}}^{\text{T}} = [\gamma_0^0,\ \ldots, \gamma_{\text{N}}^{\text{N}}]. \end{aligned} \tag{6}$$

If we wish to create specific SH coefficients $\boldsymbol{\gamma}_{\text{N}}$ with the loudspeakers, their weights should be $\boldsymbol{g} = \boldsymbol{L}_{\text{N}}^{+}\,\boldsymbol{\gamma}_{\text{N}}$, using the pseudo-inverse

of $\boldsymbol{L}_{\mathrm{N}}$. Choosing $\boldsymbol{\gamma}_{\mathrm{N}} = \boldsymbol{y}_{\mathrm{N}}(\boldsymbol{\theta})$, we obtain the sensitivity of the $\mu^{\text{th}}$ microphone interpolated in terms of SH:

$$h_\mu(\boldsymbol{\theta}, \omega) = \boldsymbol{h}_\mu^{\mathrm{T}}(\omega)\, \boldsymbol{L}_{\mathrm{N}}^{+}\, \boldsymbol{y}_{\mathrm{N}}(\boldsymbol{\theta}). \tag{7}$$

Note that here some spherical harmonics need to be excluded from the vector $\boldsymbol{y}_{\mathrm{N}}(\boldsymbol{\theta})$. Because the microphone array under test is a table-top pressure-zone array, we are given a sound-rigid acoustic boundary condition on the horizontal plane. Only the $\frac{(\mathrm{N}+1)(\mathrm{N}+2)}{2}$ even-symmetric spherical harmonics $Y_n^{2s-n}(\boldsymbol{\theta})$, $0 \le s \le n$, fulfill this condition; others are grayed out in fig.4 showing $0 \le n \le 2$. For fine interpolation, the given grid allows to choose $\mathrm{N} = 14$ at a

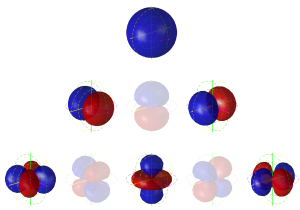

Figure 4: *SHs up to order* 2 *that satisfy the boundary condition (colored); skew symmetric are transparent.*

reasonable condition number for pseudo inversion. Figure 5 shows the three-dimensional directivity pattern of microphone 3 at about 1kHz on a fine grid of 12000 nodes.

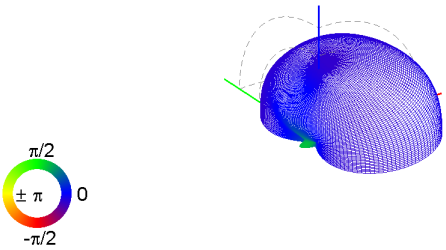


Figure 5: *SH-interpolated directivity pattern of microphone* 3 *at* $f \approx 1$kHz*; color expresses the phase.*

## 3. MODAL BEAMFORMING BY MIMO INVERSION OF MEASURED SH DIRECTIVITIES

The targeted spherical harmonic modal beamformer is shown in fig. 6. It processes the microphone signals as to produce a set of spherical harmonic pickup patterns of limited order $n$, $n \le 2$ in our particular case. This step is somewhat elegant as an output directivity can be formed by subsequent frequency-independent linear combination thereof [1].

### 3.1. Decomposer Unit

The goal is to design a unit that transforms the recorded microphone signals into the spherical harmonic spectrum $\gamma_n^m$, which are the target signals for spherical-harmonic-based modal beamforming.

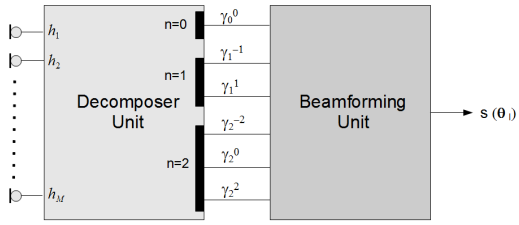


Figure 6: *Scheme of modal beamforming stages;* $s(\boldsymbol{\theta}_1)$ *denotes the output signal for a beam steered towards* $\boldsymbol{\theta}_1$.

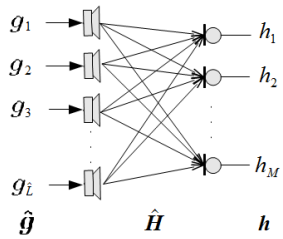


Figure 7: *MIMO system.*

The multiple-input-multiple-output system (MIMO, see fig. 7) of the device under test is described as

$$\boldsymbol{h}(\omega) = \hat{\boldsymbol{H}}(\omega)\, \hat{\boldsymbol{g}}, \tag{8}$$

where $\hat{\boldsymbol{H}}(\omega)$ represent measured MIMO responses, and $\boldsymbol{h}(\omega)$ are now all the M microphone responses due to the loudspeaker weights $\hat{\boldsymbol{g}}$. Omitting $(\omega)$ for brevity, the matrix $\hat{\boldsymbol{H}}$ contains responses from Eq. (2)

$$\hat{\boldsymbol{H}} = [\hat{\boldsymbol{h}}_1, \ldots, \hat{\boldsymbol{h}}_{\mathrm{M}}]^{\mathrm{T}}. \tag{9}$$

Hatted variables $\hat{\boldsymbol{h}}_\mu(\omega)$ are used to denote a coarse selection of measurements out of $\boldsymbol{h}_\mu(\omega)$, see red dots in fig. 2. This is preferable in practical and repeated calibration measurement, so that modal beamformer design only uses the 6 loudspeaker positions $\boldsymbol{\theta}_\mu = [\cos(\varphi_\mu)\sin(\vartheta_\mu), \sin(\varphi_\mu)\sin(\vartheta_\mu), \cos(\vartheta_\mu)]^{\mathrm{T}}$ aligned with all 6 pointing directions of the microphone array elements. The fine 288 measurement grid is only used for later verification. We control the reduced loudspeaker weights $\hat{\boldsymbol{g}}$ by the smaller $6 \times 6$ matrix $\boldsymbol{Y}^{-1}$ instead of $\boldsymbol{L}^{+}$,

$$\hat{\boldsymbol{g}} = \boldsymbol{Y}^{-1}\, \boldsymbol{\gamma}_2, \qquad \text{with } \boldsymbol{Y} = [\boldsymbol{y}_2(\boldsymbol{\theta}_1), \ldots, \boldsymbol{y}_2(\boldsymbol{\theta}_{\mathrm{M}})], \qquad \text{and } \boldsymbol{\gamma}_2 = [\gamma_0^0, \ldots, \gamma_2^2]. \tag{10}$$

Insertion in Eq. (8) transforms the loudspeaker side of the MIMO system to a modal representation of limited order $n \le 2$ resolvable by the microphones

$$\boldsymbol{h} = \hat{\boldsymbol{H}}\, \boldsymbol{Y}^{-1} \boldsymbol{\gamma}_2. \tag{11}$$

We may further transform the MIMO system $\hat{\boldsymbol{H}}$ from the microphone side into the spherical harmonics domain by using the same expression $\boldsymbol{Y}^{-1}$, yielding the modal signal outputs $\boldsymbol{\chi}_2$ of the microphone array

$$\boldsymbol{\chi}_2 = \boldsymbol{Y}^{-1}\, \hat{\boldsymbol{H}}\, \boldsymbol{Y}^{-1} \boldsymbol{\gamma}_2. \tag{12}$$

In the underlying analytical model [9], this operation would render the system

$$\boldsymbol{Y}^{-1}\, \hat{\boldsymbol{H}}\, \boldsymbol{Y}^{-1} := \boldsymbol{C} \tag{13}$$

perfectly diagonal. We therefore expect some of the paths in the $6 \times 6$ MIMO system $\boldsymbol{C}$ to be vanishing. Indeed, no perfect but a diagonalizing effect on the measured MIMO system is observed in $\boldsymbol{C}$, fig. 8. In order to obtain a correct mapping of the spherical harmonics modes at the loudspeaker side to the modes at the microphone side, a decomposition matrix that is inverse to the transformed MIMO system $\boldsymbol{C}$ is introduced

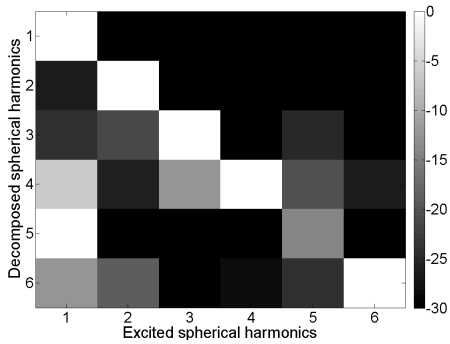


Figure 8: Magnitudes of the MIMO system $\boldsymbol{C}$ for $f = 2\,\text{kHz}$. Values are normalized to a range of 30 dB.

$$\boldsymbol{\chi}_2 = \boldsymbol{D}\,\boldsymbol{C}\,\boldsymbol{\gamma}_2 = \boldsymbol{\gamma}_2. \tag{14}$$

A decomposition matrix $\boldsymbol{D} = \boldsymbol{C}^{-1}$ would yield a perfect but non-robust decomposition of the microphone signals into the mode strengths $\boldsymbol{\chi}_2 = \boldsymbol{\gamma}_2$.

### 3.2. Regularised inversion of the transformed MIMO system

The transformed MIMO system is square and may be exactly inverted to get $\boldsymbol{D}$ if it is non-singular. The condition number $\kappa(\cdot)$ of a matrix indicates the distance to a regular matrix and is defined as the ratio between the maximal and minimal singular value [10]. A perfectly regular matrix has a condition number $\kappa(\cdot) = 1$, but we expect $\kappa(\boldsymbol{C}) > 1$ in our case. By applying the singular value decomposition (SVD, [11]) on $\boldsymbol{C}$, we obtain

$$\boldsymbol{C} = \boldsymbol{U}\,\boldsymbol{S}\,\boldsymbol{V}^{\mathrm{H}}, \tag{15}$$

where $\boldsymbol{U}$ and $\boldsymbol{V}$ are unitary matrices column-wisely containing the left and right singular vectors of $\boldsymbol{C}$, and $\boldsymbol{S}$ is the diagonal matrix containing the singular values in descending order

$$\boldsymbol{S} = \mathrm{diag}(\boldsymbol{\sigma}), \quad \boldsymbol{\sigma} = [\sigma_1, \ldots, \sigma_N]^{\mathrm{T}}. \tag{16}$$

We define a regularised inverse of the MIMO system matrix $\boldsymbol{C}$ as

$$\boldsymbol{D} = \boldsymbol{V}\tilde{\boldsymbol{S}}^{-1}\boldsymbol{U}^{\mathrm{H}}, \text{with } \tilde{\boldsymbol{S}}^{-1} = \mathrm{diag}(\tilde{\boldsymbol{\sigma}})^{-1}, \tag{17}$$

$$\text{and } \tilde{\boldsymbol{\sigma}} = \boldsymbol{\sigma} + \underbrace{\sigma_1\, c_1}_{\text{local}} + \underbrace{\sigma_{max}\, c_2}_{\text{global}}, \tag{18}$$

where $\tilde{\boldsymbol{\sigma}}$ denotes the regularised singular values, $\sigma_1$ denotes the highest singular value of the system matrix at frequency $f$ (local), $\sigma_{max} = \max_f(\sigma_1(f))$ refers to the maximal singular value over the entire frequency range (global), and $c_1, c_2$ are scalar regularisation constants. They are used to control the amount of regularisation. Local and global regularisation improve the system conditioning to obtain a robust modal decomposer $\boldsymbol{D}$. The local regularisation is used to avoid an extreme amplification of the inverse system at frequencies where just a few components are under-represented in $\boldsymbol{C}$, whereas the global regularisation avoids amplification at frequencies where transfer function components in $\boldsymbol{C}$ are too weak, altogether. Global regularisation is essential in the lower frequency range, whereas local and global regularisation affect the approximation at higher frequencies to the same extent. Fig. 9 shows that

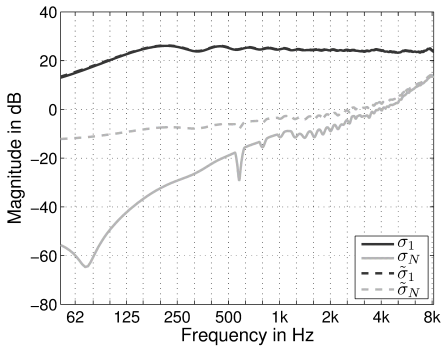


Figure 9: , *Maximal and minimal singular values of the transformed MIMO system and the regularised system for* $c_2 = 0.008$ *and* $c_1 = 0.01$.

regularisation mainly affects the small singular values to improve the robustness of $\boldsymbol{D}$ while accepting it being a less accurate inverse $\boldsymbol{D}\,\boldsymbol{C} \approx \boldsymbol{I}$.

### 3.3. Modal Beamforming Unit

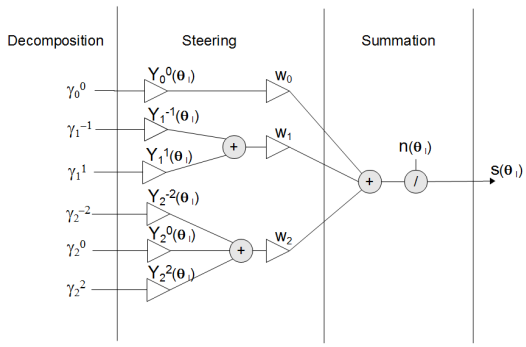


Figure 10: *Scheme of beamforming unit.*

A block diagram of the beamformer unit is depicted in fig.10. Thereby, the input signals are the unified modes in the spherical harmonics domain $\gamma_n^m$ that are generated in the decomposer unit using the MIMO filter $\boldsymbol{D}$. In the steering unit, these signals are weighted with the spherical harmonics evaluated at the lookdirection $\boldsymbol{\theta}_l$, and in a next step they are multiplied with frequency independent order weights $w_n$, e.g. the max-$r_{\mathrm{E}}$ weights $[1, 0.775, 0.4]$, that are designed to form specific beampattern shapes (see [12], [13], [14] and [9]). In the last unit, the summation unit, the obtained signals are summed up. The beampattern is normalized by its lookdirection amplitude $n(\boldsymbol{\theta}_l) = \sum_{n=0}^{2}\sum_{s=0}^{n} w_n\,[Y_n^{2s-n}(\boldsymbol{\theta}_l)]^2$ to remove its dependency on the zenith angle.

## 4. RESULTING BEAMPATTERNS

The horizontal slices of the achievable beampatterns with max-$r_{\mathrm{E}}$ order weighting $w_n = [1, 0.775, 0.4]$ steered towards the horizontal array plane are shown in fig. 11. It is striking that the

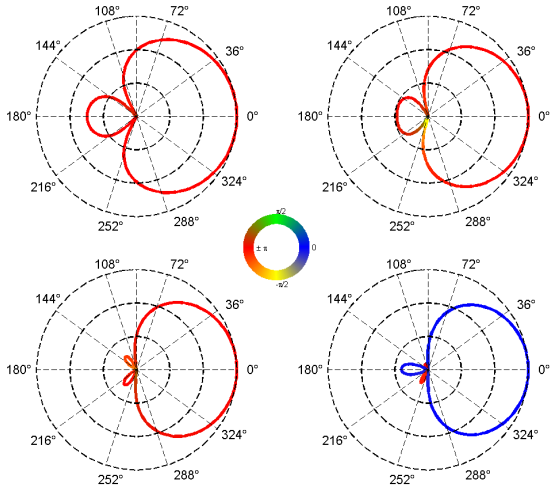


Figure 11: *Horizontal slice of supercardioid beampattern steered toward* $z = 0$ *at frequencies of* $[400, 1000, 2000, 4000]$ *Hz and usage of regularised decomposition filters; radial divisions are* 10 *dB steps.*

obtained directional characteristics are frequency dependent and that the beampatterns evolve from a nearly first order supercardioid at low frequencies to a second order supercardioid characteristic at high frequencies. The vertical slices of a hypercardioid beam ($w_n = [1, 1, 1]$) steered towards the z-direction are shown in fig. 12 where one can observe a similar behaviour as for the horizontal slices, namely that the higher order pattern is just available at higher frequencies. The quasi order-limited beamforming is caused by the

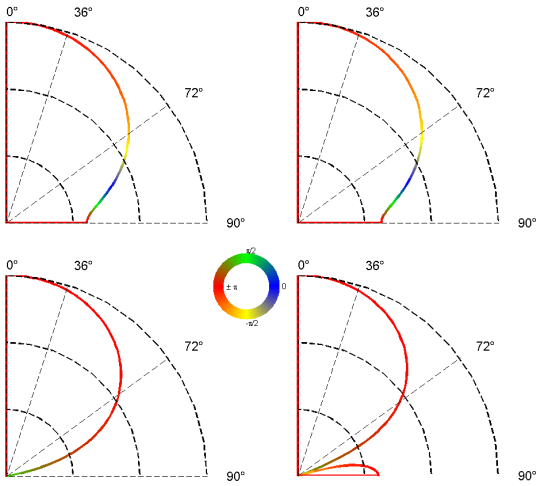


Figure 12: *Vertical slice of hypercardioid beampattern steered towards the z-direction at frequencies of* $[400, 1000, 2000, 4000]\,Hz$ *and usage of regularised filters; radial divisions are* 10 *dB steps.*

filter regularisation, as the higher-order modes are weakly present at low frequencies. This order limitation improves the white noise gain (WNG) and accordingly the robustness of the beamforming system [15].

### 4.1. Does every array need calibration?

The filters designed by limiting the condition number to $\sim$ 30dB (see fig. 9) still yield a robust decomposition if the array parameters deviate within 1%. But is the MIMO decomposer also applicable to different copies of the microphone array?

In order to test the portability of the regularised decomposition filters to an array duplicate with same geometry, we generated filters with the circularly rotated data of the measured matrix $\hat{\boldsymbol{H}}$. The beamforming system for the rotated filters was tested on the original microphone array. The obtained beampatterns of this setup highly vary from the beampatterns produced with the original data, see fig. 13. Thus, the designed filters are not necessarily applicable to arrays where the array characteristics differ from the array prototype. In [9] it is shown that minor mounting errors (about

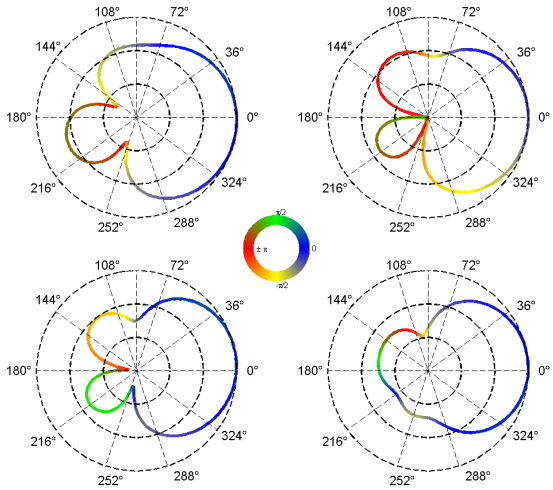


Figure 13: *Horizontal slice of supercardioid beampattern steered toward* $z = 0$ *at frequencies of* $[400, 1000, 2000, 4000]\,Hz$ *and usage of rotated regularised decomposition filters; radial divisions are* 10 *dB steps.*

$4°$) of the microphone orientation, gain mismatches between the channels as well as deviations of microphone characteristics lead to major decomposition errors. This highlights the importance of a calibration procedure for every microphone array duplicate.

## 5. CONCLUSIONS

In this paper, we presented and tested a novel modal beamforming approach for a six channel pressure-zone table-top microphone array. The design using five cardioid microphones and one omnidirectional central microphone yields robust frequency responses for creating 2nd order modal beampatterns. A measurement-based decomposition for modal beamforming that exploits the benefits of gradient transducers of reasonable manufacturing accuracy is proposed. The practical approach includes a regularised inversion of a MIMO system and is easy to use as only $6 \times 6$ MIMO response

measurements are necessary. The low complexity of this calibration procedure is paramount as exchangeability of the MIMO decomposition filters to array duplicates is not possible for superdirectional beamforming.

## 6. ACKNOWLEDGMENTS

We want to thank Dominik Biba, Martin Opitz, Richard Pribyl, and Marco Riemann from AKG Acoustics GmbH for the excellent collaboration and for building the microphone array prototype within the project AAP, which was funded by the Austrian ministries BMVIT, BMWFJ, the Styrian Business Agency (SFG), and the departments 3 and 14 of the Styrian Government. The Austrian Research Promotion Agency (FFG) conducted the funding under the Competence Centers for Excellent Technologies (COMET, K-Project), a program of the above mentioned institutions. Further we want to thank Hannes Pomberger (IEM) for co-developing design and algorithm of the presented pressure-zone table-top microphone array.

## 7. REFERENCES

[1] J. Meyer and G. Elko, "A highly scalable spherical microphone array based on an orthonormal decomposition of the soundfield," in *Acoustics, Speech, and Signal Processing (ICASSP), 2002 IEEE International Conference on*. IEEE, 2002, vol. 2, pp. II–1781.

[2] Heinz Teutsch, *Modal array signal processing: principles and applications of acoustic wavefield decomposition*, vol. 348, Springer, 2007.

[3] Z. Li and R. Ruraiswami, "Hemispherical microphone arrays for sound capture and beamforming," in *Applications of Signal Processing to Audio and Acoustics, 2005. IEEE Workshop on*. IEEE, 2005, pp. 106–109.

[4] F. Reining, "Microphone arrangement comprising pressure gradient transducers," Feb. 23 2009, US Patent App. 12/390,990.

[5] J. Meyer and G. Elko, "Spherical harmonic modal beamforming for an augmented circular microphone array," in *Acoustics, Speech and Signal Processing, 2008. ICASSP 2008. IEEE International Conference on*. IEEE, 2008, pp. 5280–5283.

[6] J.M. Meyer and G.W. Elko, "Augmented elliptical microphone array," July 9 2008, US Patent App. 12/595,082.

[7] Peter G. Craven, Malcolm Law, and Chris Travis, "Microphone array," 2008, Patent App. WO 2008/040991 A2.

[8] A. Farina, "Simultaneous measurement of impulse response and distortion with a swept-sine technique," *Preprints-Audio Engineering Society*, 2000.

[9] Markus Zaunschirm, "Modal beamforming using planar circular microphone arrays," M.S. thesis, University of Music and Performing Arts Graz, 2012.

[10] E.W. Cheney and D.R. Kincaid, *Numerical mathematics and computing*, Brooks/Cole Pub Co, 2007.

[11] J.E. Jackson and J. Wiley, *A user's guide to principal components*, Wiley Online Library, 1991.

[12] J. Daniel, J.B. Rault, and J.D. Polack, "Ambisonics encoding of other audio formats for multiple listening conditions," *PREPRINTS-AUDIO ENGINEERING SOCIETY*, 1998.

[13] Gary W. Elko, "Differential microphone arrays," in *Audio signal processing for next-generation multimedia communication systems*, Yiteng Arden Huang and Jacob Benesty, Eds. Springer, 2004.

[14] Gary W. Elko, "Superdirectional microphone arrays," in *Acoustic signal processing for telecommunication*, Steven L Gay and Jacob Benesty, Eds. Kluwer Academic, 2000.

[15] G.W. Elko, R.A. Kubli, J.M. Meyer, et al., "Audio system based on at least second-order eigenbeams," Sept. 8 2009, US Patent 7,587,054.